Pcdhβ deficiency affects hippocampal CA1 ensemble activity and contextual fear discrimination

Hirotaka Asai[1,2], Noriaki Ohkawa[1,2,3], Yoshito Saitoh[1,2,3], Khaled Ghandour[1,2], Emi Murayama[1,2], Hirofumi Nishizono[4], Mina Matsuo[4], Teruyoshi Hirayama[5], Ryosuke Kaneko[6], Shin-ichi Muramatsu[7,8], Takeshi Yagi[9] and Kaoru Inokuchi[1,2]*

Abstract

Clustered protocadherins (Pcdhs), a large group of adhesion molecules, are important for axonal projections and dendritic spread, but little is known about how they influence neuronal activity. The Pcdhβ cluster is strongly expressed in the hippocampus, and in vivo Ca^{2+} imaging in Pcdhβ-deficient mice revealed altered activity of neuronal ensembles but not of individual cells in this region in freely moving animals. Specifically, Pcdhβ deficiency increased the number of large-size neuronal ensembles and the proportion of cells shared between ensembles. Furthermore, Pcdhβ-deficient mice exhibited reduced repetitive neuronal population activity during exploration of a novel context and were less able to discriminate contexts in a contextual fear conditioning paradigm. These results suggest that one function of Pcdhβs is to modulate neural ensemble activity in the hippocampus to promote context discrimination.

Keywords: Hippocampus, CA1, Clustered protocadherin, Pcdhβ, Ca^{2+} imaging, Ensemble, Contextual fear memory, Discrimination

Introduction

Clustered protocadherins (Pcdhs) are a large group of adhesion molecules important for axonal projections and dendritic spread [1–6]. Pcdhs comprise three subgroups, Pcdhα, Pcdhβ, and Pcdhγ, expressed as 58 isoforms in mice [7]. These molecules impart two unique characteristics: each cell can express one of diverse combinations of isoforms, and the isoforms have highly specific homophilic interactions with each other [8]. Pcdhs contribute to serotonergic axonal tiling in the hippocampus, axonal projections in the olfactory bulb, dendritic self-avoidance, and dendritic spread in the retina and the cortex [1–6, 9]. However, it is not clear whether these largely morphological effects impact neuronal activity.

Pcdhαs and Pcdhγs have extracellular and intracellular domains, whereas Pcdhβs have only extracellular domains [10]. Pcdhβs are strongly expressed in the olfactory bulb [11], influencing axonal targeting during embryonic stage [12], as well as in the hippocampus, a brain region in which synchronous, or ensemble, activity of neurons enables learning and memory [13, 14]. However, whether Pcdhβs affect ensemble activity in the hippocampus is not known. Of note, synchronous activity is regulated by inhibitory GABAergic neurons [15, 16], and the loss of Pcdhβs was shown to affect the survival of spinal inhibitory neurons during embryonic stage [12].

Here, we investigated neural activity in the hippocampi of Pcdhβ-deficient mice. In vivo Ca^{2+} imaging revealed that a loss of Pcdhβ induced distinctive neural ensemble activity in the CA1 region during context exploration. This resulted in impaired contextual discrimination during behavioral experiments involving fear conditioning.

* Correspondence: inokuchi@med.u-toyama.ac.jp
[1]Department of Biochemistry, Graduate School of Medicine and Pharmaceutical Sciences, University of Toyama, Toyama 930-0194, Japan
[2]Core Research for Evolutional Science and Technology (CREST), Japan Science and Technology Agency (JST), University of Toyama, Toyama 930-0194, Japan
Full list of author information is available at the end of the article

Results

Pcdhβ deficiency reduces population activity in hippocampal CA1

To investigate the effect of Pcdhβ deletion on hippocampal neuronal activity, we performed Ca^{2+} imaging experiments in freely moving wild-type (Wt) and Pcdhβ-deficient (Δβ) mice (Fig. 1a). For this, neurons in CA1 were infected with adeno-associated viruses (AAVs) encoding calcium indicator G-CaMP7 under the control of the CaMKII promoter for expression by excitatory neurons, and the mice were fitted with a head-mount miniature fluorescence microscope [14, 17, 18] (Fig. 1b). Ca^{2+} imaging was performed while mice were in their home cage (pre) and during contextual exploration (sq) sessions [14, 19] (Fig. 1c). Acquired images were then processed and analyzed as described previously [14] (see Additional file 1: Figure S1). Correlation matrix analysis (Fig. 1d) showed that repetitive neuronal activity in Δβ mice was reduced during sq. sessions compared with that in Wt mice at different time points (Fig. 1e–f). The sum of the correlations during contextual exploration (sq-sq) was significantly lower in Δβ mice than in Wt mice (Fig. 1g; adjusted P-value (P_{adj}) = 0.0013 by Bonferroni's multiple-comparison test). However, no significant difference in the repetitive correlation activity was observed either in home cage (pre-pre) sessions or between home cage and context exposure (pre-sq) sessions in Δβ or Wt mice (Fig. 1g; P_{adj} = 0.1838 for pre-pre, P_{adj} = 0.2583 for pre-sq by Bonferroni's multiple-comparison test). The difference observed during contextual exploration was not due to their difference of behavioral activity in both genotypes because their behavioral activity was equivalent in open field task (Additional file 2: Figure S2). Moreover, there were no significant differences between Wt and Δβ mice at the individual cell level regarding the number of observed Ca^{2+} events or ratios of sq./pre Ca^{2+} events (Additional file 3: Figure S3). These results suggest that Pcdhβ deficiency reduces repetitive synchronous activity in the CA1 at the population level but not at the cellular level during contextual exploration.

Pcdhβ deficiency modulates ensemble activity in CA1

To further study the effect of Pcdhβ deletion on population activity, we used non-negative matrix factorization (NMF) to analyze ensembles of collectively firing neurons [14] (Additional file 4: Figure S4a–b). The normalized number of total ensembles extracted by NMF was similar between Wt and Δβ mice in both pre and sq sessions (Additional file 4: Figure S4c–d). The number of ensembles comprising 20 or more cells, defined here as large ensembles, was larger in Δβ mice than in Wt mice (Fig. 2a–d; Additional file 5: Figure S5). However, these large ensembles were seldomly activated (Additional file

5: Figure S5). Although the number of activated cells were similar between the genotypes (Additional file 1: Figure S1c), larger portion of cells was shared across the ensembles in Δβ mice than in Wt mice in both sessions (Fig. 2e–f). These results demonstrate that Pcdhβs modulate ensemble size and composition in hippocampal CA1.

### Pcdhβ deficiency impairs context discrimination during fear conditioning

As Pcdhβ deficiency altered neuronal activity in the hippocampus, we investigated the effect on hippocampus-dependent memory function with contextual fear conditioning task [20] (Fig. 3a). Pcdhβ-deletion and Wt mice showed comparable levels of freezing in the conditioned context (Fig. 3b; square: $F_{(21, 18)}$ = 2.140, P = 0.1080; t_{39} = 1.141, P = 0. 2607; unpaired t-test). However, the discrimination efficiency between the conditioned context (square) and a novel context (circle) was significantly impaired in Δβ mice compared with that in Wt mice (Fig. 3c; $F_{(18, 21)}$ = 1.645, P = 0.2737; t_{39} = 2.310, P = 0.0263; unpaired t-test). These results suggest that Pcdhβs play a key role in the specificity of memories and in discriminating between events, which is consistent with the formation of ensembles with more shared cells in Δβ mice than in Wt mice.

Discussion

In this study, we showed that Pcdhβs contribute to the organization of neuronal ensembles in the hippocampus of freely moving mice. These findings extend what was previously shown regarding the role of Pcdhs in regulating neuronal morphology [1–5]. Interestingly, we found that Pcdhβ regulates neuronal activity at the population level but not at the cellular level. Specifically, Pcdhβ deficiency resulted in larger ensembles in CA1 and larger proportion of neurons shared between ensembles, thereby reducing their ensemble diversity. This supports the hypothesis that Pcdhs are important for the formation of diverse assembly based on the multitude of possible combinations of isoforms, which have highly specific homophilic interactions [21]. Furthermore, the large ensembles in Δβ mice were rarely activated (Additional file 5: Figure S5). These results are consistent with those from an in vitro study showing that complete deletion of Pcdhs (including α, β, and γ isoforms) induces large-amplitude low-frequency synchronous Ca^{2+} activity [22]. Thus, Pcdhβs are important for the diversity of neuronal activity in the hippocampus.

The altered ensemble activity in the hippocampi of Δβ mice resulted in an impaired ability to discriminate contexts in a fear conditioning memory task without
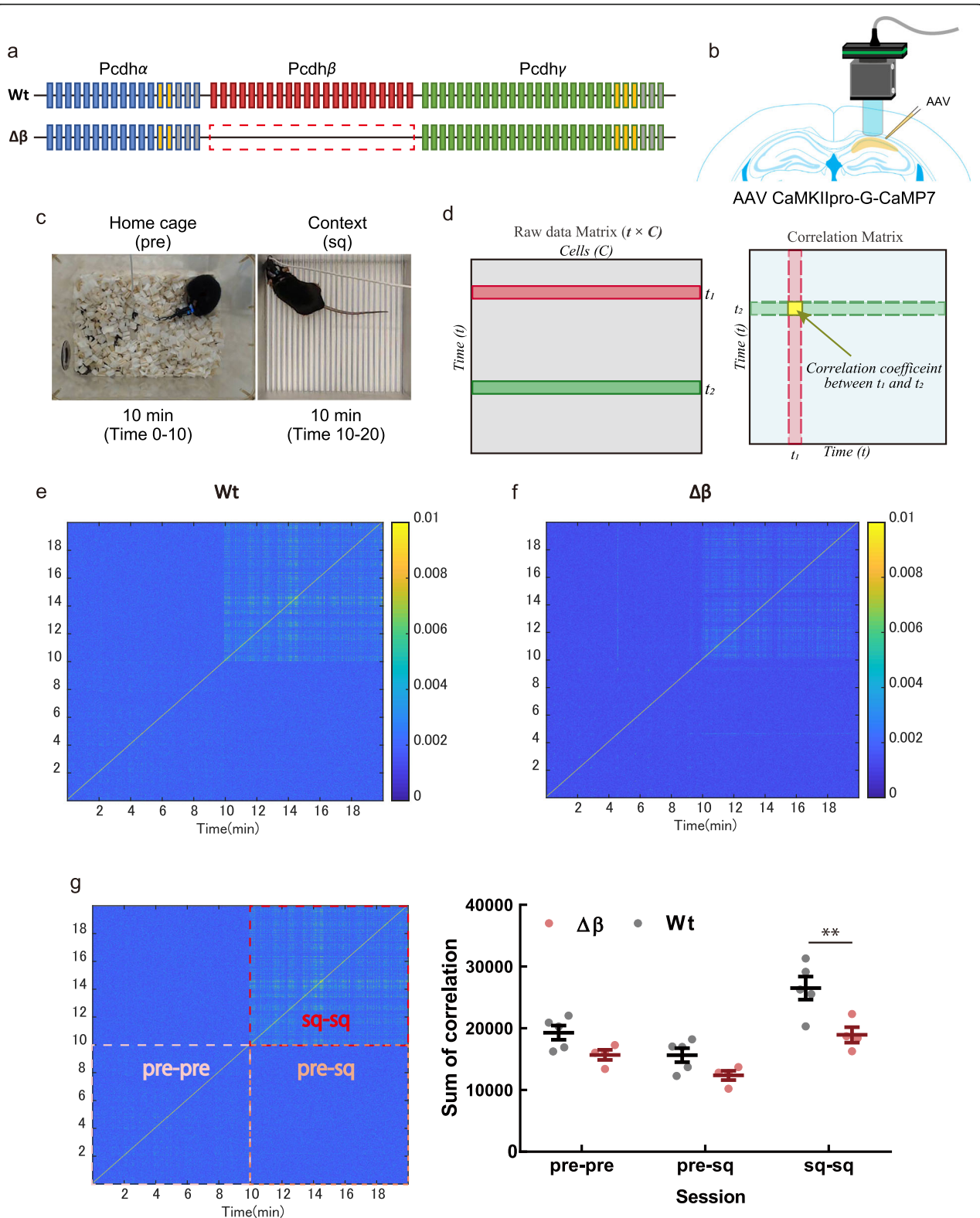
Fig. 1 Pcdhβ deficiency reduces repetitive neuronal activity in the hippocampus. **a** Pcdhβ deletion. **b** Induction of CaMKII-G-CaMP7 by AAV and implantation of GRIN lens over the right hippocampal CA1 region. **c** Ca^{2+} imaging in home cage (pre) and square context (sq). **d** Schematic of the correlation matrix analysis. Representative images of correlation matrices for activation in Wt (**e**) and Δβ (**f**) mice. **g** Summation of correlation coefficients between sessions ($n = 5$ Wt mice, 4 Δβ mice). Data are means ± standard errors of the means (SEMs). **$P < 0.01$ (adjusted P-value from Bonferroni's multiple-comparison test)
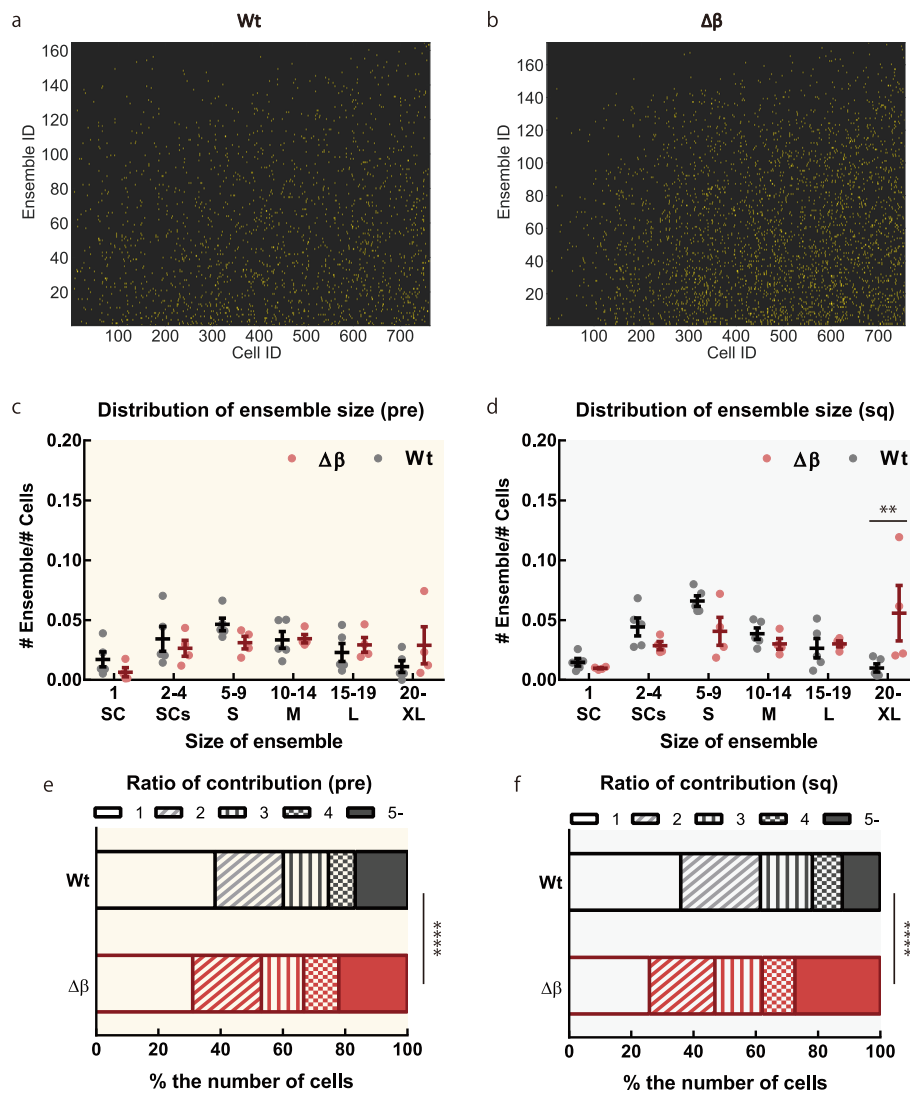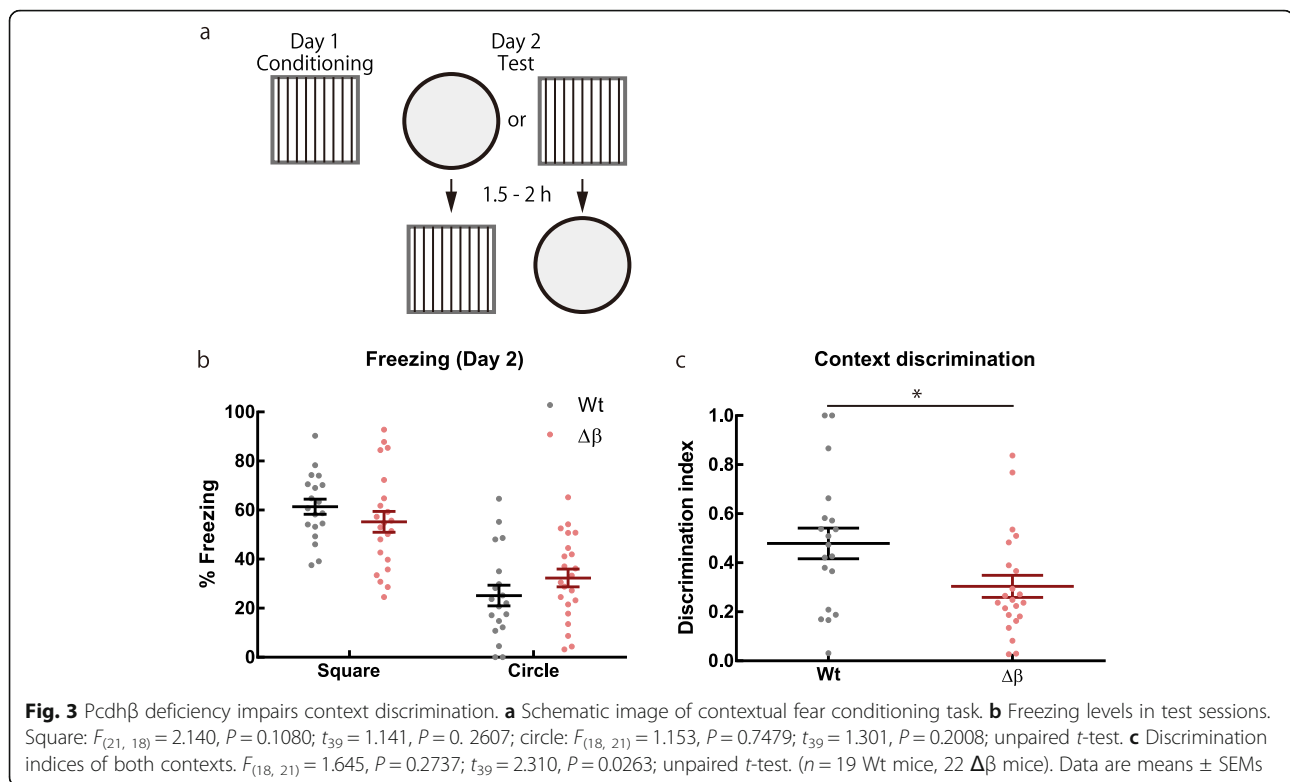
Fig. 2 Pcdhβ deficiency affects ensemble size and the proportion of neurons shared between ensembles. Representative images of binarized basis matrices from Wt (**a**) and Δβ (**b**) mice. Yellow dots represent the cells contributing to the ensemble. **c–d** Normalized number of ensembles according to ensemble size. Statistical values from Bonferroni's multiple-comparison test are provided in Additional file 6: Table S1 ($n = 5$ Wt mice, 4 Δβ mice). Data are means ± SEMs. **$P < 0.01$ (adjusted P-value from Bonferroni's multiple-comparison test). Percentages of neuronal cells contributing to one ensemble (open bars) and multiple ensembles (pattern and solid bars) in Wt and Δβ mice during pre (**e**) and sq (**f**) sessions. ****$P < 0.0001$ (chi-square test)

affecting their ability to learn the association. This is consistent with previous reports showing that spatial memory was not impaired in Pcdh-mutant mice [3, 23], although Pcdhα was important for high load memory tasks [24]. The impairment of context discrimination exhibited by the Δβ mice may be attributed to the increased sharing of cells between ensembles. As previously reported, a set of neurons or ensemble has specific information [25, 26]. These can support our interpretation that low independence of neuronal composition between ensembles in Δβ mice will lead the inability to process distinguish information about two contexts.

Nevertheless, it still remains an open question how neurons are selected in allocating information. Collectively, the evidence suggests that Pcdhs play an important role in higher brain function such as context discrimination.

In summary, the data presented here demonstrate that Pcdhβs tune ensemble activities in the CA1 area of the hippocampus. Our results suggest that this ensemble activity contributes to contextual discrimination. The findings that Pcdhs configure functional ensembles helps to elucidate the mechanisms underlying the processing of information in the mammalian brain.

Fig. 3 Pcdhβ deficiency impairs context discrimination. **a** Schematic image of contextual fear conditioning task. **b** Freezing levels in test sessions. Square: $F_{(21, 18)} = 2.140$, $P = 0.1080$; $t_{39} = 1.141$, $P = 0.2607$; circle: $F_{(18, 21)} = 1.153$, $P = 0.7479$; $t_{39} = 1.301$, $P = 0.2008$; unpaired *t*-test. **c** Discrimination indices of both contexts. $F_{(18, 21)} = 1.645$, $P = 0.2737$; $t_{39} = 2.310$, $P = 0.0263$; unpaired *t*-test. ($n = 19$ Wt mice, 22 **Δ**β mice). Data are means ± SEMs

Methods

Animals

The generation of Δβ mice was described previously [12]. Briefly, in vitro fertilization and embryo transfer techniques were performed using heterozygous male and female mice [19]. Genotypes were determined from tail DNA samples by PCR using primers TTGTGAGTGC TCCATAGCCTC, GCTCCTGATTGAATTTGCC, and TGATGTGGGTCTGGTTTCC with conditions of 95 °C for 3 min, 30 cycles of 95 °C for 15 s, 60 °C for 15 s, 72 °C for 45 s, and 72 °C for 2 min. The resulting PCR products were 519 bp for Wt and 626 bp for Δβ mice.

The mice were housed under a 12 h light/dark cycle (lights on, 7:00 am) at 24 °C ± 3 °C and 55% ± 5% humidity with ad libitum access to food and water. All animal experiments were conducted in accordance with the guidelines of the National Institutes of Health (NIH) and were approved by the Animal Care and Use Committee of the University of Toyama.

AAV constructs

The pAAV-CaMKII-G-CaMP7 plasmid was constructed by replacing C1V1-mCherry from pAAV-CaMKII-C1V1-mCherry plasmid (donated by Dr. Karl Deisseroth) with the G-CaMP7 sequence from pN1-G-CaMP7 plasmid [27, 28] using the BamHI and EcoRI sites of pAAV-CaMKII-C1V1-mCherry, and the BglII and NotI sites of pN1-G-CaMP7. The resulting pAAV-CaMKII-

G-CaMP7 plasmid was prepared using an EndoFree Plasmid Maxi kit (Qiagen). The recombinant AAV vectors were produced as described previously [29, 30] to obtain a viral titer of 9.4×10^{12} vg/mL. The virus was diluted 40-fold in phosphate-buffered saline for injections into mice.

Stereotactic surgery

Male Δβ mice and Wt littermates (at least 12 weeks old) were anesthetized with pentobarbital (64.8 mg/kg of body weight, intraperitoneally (i.p.)) or a combination anesthetic (0.75 mg/kg, i.p., medetomidine (Domitor; Nippon Zenyaku Kogyo Co., Ltd., Japan), 4.0 mg/kg, i.p., midazolam (Fuji Pharma Co., Ltd., Japan), and 5.0 mg/ kg, i.p., butorphanol (Vetorphale, Meiji Seika Pharma Co., Ltd., Japan) [31]) and were then placed in a stereotactic apparatus (Narishige, Japan). AAV (0.3 μL) was injected into the right CA1 (2.0 mm posterior and 1.5 mm lateral to bregma, 1.45 mm below the dura) at a rate of 0.5 μL/min using a mineral oil-filled glass micropipette connected to an IMS-20 (Narishige). The glass micropipette was kept at the target site for an additional 3 min before being withdrawn. Animals anesthetized with combination anesthetic were given an injection of atipamezole (1.5 mg/kg, intramuscularly (Antisedan; Nippon Zenyaku Kogyo Co., Japan)), an antagonist of medetomidine, to promote recovery from the anesthesia.

Asai *et al. Molecular Brain*   (2020) 13:7

Page 6 of 10

At least 2 weeks after AAV injection, a gradient index (GRIN) lens was implanted in each mouse as described previously [14, 17, 18, 32]. Mice were anesthetized as described above and placed in a stereotactic apparatus. A craniotomy (2.0 mm diameter) was performed centered over the injection site, and the neocortex and corpus callosum above the alveus overlying the dorsal hippocampal CA1 were aspirated under constant irrigation with saline using a 26-gauge flat-tip needle. Saline was applied to control the bleeding, and the GRIN lens (1 mm diameter, 4 mm length; Inscopix, Inc., USA) was placed on the alveus and depressed an additional 10–30 μm using handmade forceps attached to a manipulator (Narishige). Bone wax melted by a low-temperature cautery was applied to seal any gaps between the skull edge and the GRIN lens, and the lens was cemented in place. Five to seven anchor screws were placed in the skull for reinforcement. After the surgery, Ringer's solution (0.7 mL/mouse, i.p.; Otsuka, Japan) was injected, and atipamezole was administered as described above. Mice were maintained in individual cages after the surgery.

At least 3 weeks after GRIN implantation, surgery to set a baseplate (Inscopix, Inc.) was performed as described previously [14, 17]. Briefly, anesthetized mice were placed in a stereotactic apparatus, and a baseplate attached to a miniature microscope (nVista HD v2; Inscopix, Inc.) set at the middle of its focal range was arranged using Gripper (Inscopix, Inc.); the optimal location was determined according to blood vessels as cues. The baseplate was cemented to the cement over the skull at 5–20 μm above the optimal location. Atipamezole was administered to mice receiving the combination anesthetic, and the baseplate cover (Inscopix, Inc.) was placed over the GRIN lens until Ca^{2+} imaging was performed.

Ca^{2+} imaging

Six days or more after setting the baseplate, mice were habituated to the experimental room for at least 1 day. Mice were lightly anesthetized with isoflurane to mount the miniature microscope. When the mice became quiet (resting state) at least 30 min after their recovery from the anesthesia, Ca^{2+} imaging was performed while the mice were in their home cage (habituation session). The imaging data were acquired for 10 min, and the microscope was detached after an additional 10 min. On the following day, Ca^{2+} imaging was similarly performed in the home cage (pre session) followed by Ca^{2+} imaging for 10 min in a novel square context (Muromachi Kikai, Co., Ltd., Japan; sq. session). The mice were then returned to their home cage (see Fig. 1b).

The square context had a Plexiglass front, gray sides, and back walls (width × depth × height: 175 mm × 165

mm × 400 mm), and the chamber floors comprised 26 stainless steel rods (2 mm diameter) placed 5 mm apart.

Calcium imaging was performed during the light cycle. Imaging data were acquired using nVista acquisition software (Inscopix, Inc.) at 1440 × 1280 pixels, at 20 frames/s, maximum gain and at optimal LED power (based on the histogram, according to the nVista user guide).

Data acquisition, preprocessing, and cell identification

Calcium transients recorded by nVista acquisition software were processed with Mosaic software (Inscopix, Inc.) as described previously [14, 33]. First, each session movie was spatially downsampled and smoothed by a factor of 2. Motion correction was performed (correction type, translation only; spatial mean ($r = 20$ pixels) subtracted, and spatial mean applied ($r = 5$ pixels)) using blood vessels as a landmark to maintain the same field of view and to correct for motion artefacts across sessions using an identical reference frame. The movie was processed with Fiji software (NIH) to remove noise. Each session movie was low-pass filtered ($r = 20$ pixels).

Each session movie was cropped at the same coordinates, and the fluorescence intensity change ($\Delta F/F$) was calculated by Mosaic as follows: $\Delta F/F = (F - F_m)/F_m$, where F is the fluorescence from an individual frame of the movie and F_m is mean fluorescence for the entire movie for that session. These resultant $\Delta F/F$ movies were concatenated. Finally, cell identification was conducted with HOTARU, an automatic sorting system, as previously reported [14, 34, 35]. The HOTARU output data matrix ($\hat{D}$; time × neuron) represents Ca^{2+} activity in each time frame for every cell.

Data analysis
Correlation matrix
To investigate repetitive synchronous activity, temporal correlation was calculated as described previously [14, 36]. Briefly, the Ca^{2+} intensity matrix ($\hat{D}$) was binned every four frames (200 ms), and then the correlation was calculated using five binned frames (1 s) as a sliding time window. For comparison between genotypes, the correlation matrix was summed every session (pre-pre, pre-sq, and sq-sq), as shown in Fig. 1g.

NMF
To extract ensemble activity, NMF was applied to the data matrix every session as described previously [14, 37, 38]. Briefly, $\hat{D}$ was binned every four frames (200 ms), and then NMF was adapted. As a result, $\hat{D}$ was optimally factorized into basis matrix ($\hat{B}$; neural ensemble matrix, ensemble × neuron) and the corresponding occurrence matrix ($\hat{C}$; occurrence matrix, time × ensemble), $\hat{D} \approx \hat{B}\hat{C}$. Here, $\hat{B}$ rep-

Asai *et al. Molecular Brain*   (2020) 13:7

Page 7 of 10

resents neuronal ensembles activated synchronously, and $\hat{C}$ represents the temporal activation intensity of the corresponding ensembles. To determine the optimal number of ensembles, the Akaike information criterion with second-order correction was used. To find the optimal factorization, the ensemble (basis) matrix and intensity (occurrence) matrix minimizing the cost function, defined by $E \equiv \Sigma_{ij}(D_{ij} - \Sigma_k B_{ik}C_{kj})^2$, were chosen to be the best factorization when random initial entries from matrices $\hat{B}$ and $\hat{C}$ were used for 1000 attempts at minimization.

For quantification, the number of ensembles were normalized by dividing the number of cells in each mouse to minimize the effect of the number of cells on the number of ensembles. For $\hat{B}$ and $\hat{C}$, contributing neurons and the active time of each ensemble were judged on the basis of the z-score in each ensemble (≥2 standard deviations (SDs) for contribution, ≥3 SDs for active time).

For quantification of activity at the cellular level, Ca^{2+} events were judged as activity ≥3 SDs for the entire session.

Contextual fear conditioning

Male mice 12–19 weeks old were individually housed in a room adjacent to the testing room at least 7 days before behavioral experiments. Behavioral experiments were conducted during the light cycle by investigators blinded to the genotypes of the mice. Both genotypes of mice were run in parallel. For conditioning (day 1), mice were placed in a square context (context A) and were allowed to explore freely for 148 s. Then, three foot shocks (0.4 mA, 2 s duration, 1 min apart) were applied to the chamber floor grid. One minute after the last foot shock, the mice were returned to the home cages. In the test session (day 2), mice were placed in context A or context B (circle context) for 3 min; 1.5–2 h later they were placed in the other context for 3 min. A video tracking system (Muromachi Kikai Co., Ltd.) was used to measure the freezing response, in which the motion threshold was < 10 for at least 1.5 s. Discrimination indexes were calculated as follows [39]: (freezing in context A − freezing in context B)/(freezing in context A + freezing in context B).

The behavioral equipment was described previously ([14, 19, 20]). Context A was the square context described for Ca^{2+} imaging. Context B was a black cylindrical chamber (185 mm diameter, 220 mm height) with a white acrylic floor. Overhead room lights lit both contexts, and background noise was provided by a fan inside the room. The equipment was cleaned with 80% ethanol before each exposure. A white container was used to transfer mice between the room they were housed in and the experimental room for exposure to context B.

Open field test

Male mice 12–19 weeks old were individually housed in a room adjacent to the testing room at least 7 days before behavioral experiments. Behavioral experiments were conducted during the light cycle by investigators blinded to the genotypes of the mice. Both genotypes of mice were run in parallel.

The mice were transported from the maintenance room to the experimental room and left undisturbed for at least 30 min. They were placed in open field box for 30 min. A tracking software, DuoMouse (National Institute of Genetics) [40], was used to measure their center of mass and pixel change between frames [41]. The open field box (width × depth × height: 500 mm × 500 mm × 300 mm) was with a white acrylic floor and a side wall and side walls with different pattern. Background noise was provided by a fan inside the room. The equipment was cleaned with 80% ethanol before each exposure.

Statistical analysis

Statistical analyses were performed in GraphPad Prism 6 (GraphPad Software) and MATLAB (MathWorks). Data analyses were performed with Student's *t*-tests, Bonferroni's multiple-comparison tests, chi-square tests, and Kolmogorov–Smirnov tests, as appropriate. A *P*-value < 0.05 was considered significant.

Supplementary information

Additional file 1: Figure S1. Pcdhβ deficiency does not affect the number of cells activated during recording (related to Figs. 1 and 2). (a) Flowchart of Ca^{2+} imaging data analysis. (b) Representative image and traces of identified cells. (c) Number of cells observed in the entire session. n.s.: not significant (unpaired *t*-test). $F_{(3, 4)} = 1.087$, $P = 0.9005$; $t_7 = 2.202$, $P = 0.0635$ ($n = 5$ Wt mice, 4 Δβ mice). Data are means ± SEMs.

Additional file 2: Figure S2. Behavioral activity was equivalent in open field task. (a) Open field box. (b) Traces of center of mass. Travel distance (c) and motility (d). Panel c: $F_{(25, 27)} = 3.434$, $P = 0.0023$; $t_{37.73} = 0.1515$, $P = 0.880$; panel d: $F_{(25, 27)} = 4.253$, $P = 0.0004$; $t_{35.54} = 0.2776$, $P = 0.783$; unpaired *t*-test with Welch's correction; $n = 26$ Wt mice, 28 Δβ mice. Data are means ± SEMs.

Additional file 3: Figure S3. Pcdhβ deficiency does not affect neural activity at the cellular level (related to Figs. 1 and 2, and additional file 1). (a–b) Representative images of raster plots of all recorded cells from Wt (a) and Δβ (b) mice. (c) Cumulative curve of proportion of cells against number of active events during entire recording session (pre 10 min + sq 10 min). Proportions of cells according to the number of Ca^{2+} events during pre (d) and sq (e) sessions. Statistical values from Bonferroni's multiple-comparison test are provided in Additional file 6. (f) The ratios of the number of Ca^{2+} events during the sq session to that in the pre session. Statistical values from Bonferroni's multiple-comparison test are provided in Additional file 6 ($n = 5$ Wt mice, 4 Δβ mice). Data are means ± SEMs. No significant differences were observed (Kolmogorov–Smirnov test for panel c, Bonferroni's multiple-comparison tests for panels d–f).

Additional file 4: Figure S4. Pcdhβ deficiency does not affect the number of ensembles activated in the home cage and during novel context exploration (related to Fig. 2). (a) Schematic diagram of the non-negative matrix factorization (NMF) analysis. (b) Representative image of

Asai *et al. Molecular Brain*   (2020) 13:7

Page 8 of 10

an ensemble extracted with NMF. Red arrows (left) indicate the cells contributing to this ensemble. Red dots (right) indicate the times at which the ensemble was activated. (c–d) Normalized number of ensembles extracted in each session (panel c: $F_{(4, 3)} = 1.907$, $P = 0.6229$; $t_7 = 1.648$, $P = 0.1434$; panel d: $F_{(4, 3)} = 1.086$, $P = 0.9856$; $t_7 = 0.2852$, $P = 0.7837$; unpaired *t*-test; $n = 5$ Wt mice, 4 Δβ mice). Data are means ± SEMs.

Additional file 5: Figure S5. Large ensembles are infrequently activated. Number of ensemble events during pre and sq sessions in extra-large ensembles (XL; 20 or more cells; a–b), large ensembles (L; 15–19 cells; c–d), medium ensembles (M; 10–14 cells; e–f), and small ensembles (S; 5–9 cells; g–h). Number of ensemble events during pre and sq. sessions in ensembles composed of several cells (SCs; 2–4 cells; i–j) and of single cells (SC; k–l). Statistical values from Bonferroni's multiple-comparison tests are provided in Additional file 6 ($n = 5$ Wt mice, 4 Δβ mice). Data are means ± SEMs. *$P < 0.05$ (adjusted P-value from Bonferroni's multiple-comparison test).

Additional file 6 Table S1. Tables of statistical values. *P*-values by statistical analysis of all figures and additional files.

Abbreviations
AAV: Adeno-associated virus; NMF: Non-negative matrix factorization; Pcdh: Clustered protocadherin; SD: Standard deviation; SEM: Standard error of the mean; Wt: Wild type; Δβ: Pcdhβ deficient

Authors' contributions
HA and KI designed the study. HA conducted surgeries, Ca^{2+} imaging, behavioral experiments, immunostaining, and analysis of all data. NO, YS, and KG established the Ca^{2+} imaging. EM constructed the plasmids. SM prepared the AAV. TH, RK, and TY established the Pcdhβ-deficient mice. HN and MM generated and maintained the transgenic animals. KI supervised the entire project. HA, KG, and KI wrote the manuscript. All authors read and approved the final manuscript.

Authors' information
Noriaki Ohkawa.
Present address: Division for Memory and Cognitive Function, Research Center for Advanced Medical Science, Comprehensive Research Facilities for Advanced Medical Science, Dokkyo Medical University, Tochigi 321–0293, Japan.
Yoshito Saitoh.
Present address: Division for Memory and Cognitive Function, Research Center for Advanced Medical Science, Comprehensive Research Facilities for Advanced Medical Science, Dokkyo Medical University, Tochigi 321–0293, Japan.

Availability of data and materials
The datasets used and/or analyzed during the current study are available from the corresponding author on reasonable request.

Ethics approval and consent to participate
All procedures involving the use of animals complied with the guidelines of the National Institutes of Health and were approved by the Animal Care and Use Committee of the University of Toyama.

Consent for publication
Not applicable.

Competing interests
SM owns equity in a company (Gene Therapy Research Institution) that commercializes the use of AAV vectors for gene therapy applications. To the extent that the work in this manuscript increases the value of these commercial holdings, SM has a conflict of interest. The other authors declare that they have no competing interests.

Author details
[1]Department of Biochemistry, Graduate School of Medicine and Pharmaceutical Sciences, University of Toyama, Toyama 930-0194, Japan. [2]Core Research for Evolutional Science and Technology (CREST), Japan Science and Technology Agency (JST), University of Toyama, Toyama 930-0194, Japan. [3]Precursory Research for Embryonic Science and Technology (PRESTO), JST, Saitama 332-0012, Japan. [4]Division of Animal Experimental Laboratory, Life Science Research Center, University of Toyama, Toyama 930-0194, Japan. [5]Department of Anatomy and Developmental Neurobiology, Tokushima University, Tokushima 770-8501, Japan. [6]Bioresource Center, Gunma University Graduate School of Medicine, Gunma 371-8511, Japan. [7]Division of Neurology, Department of Medicine, Jichi Medical University, Tochigi 329-0498, Japan. [8]Center for Gene and Cell Therapy, The Institute of Medical Science, The University of Tokyo, Tokyo 108-8639, Japan. [9]KOKORO-Biology Group, Laboratories for Integrated Biology, Graduate School of Frontier Biosciences, Osaka University, Osaka 565-0871, Japan.

References
1. Katori S, Hamada S, Noguchi Y, Fukuda E, Yamamoto T, Yamamoto H, et al. Protocadherin-alpha family is required for serotonergic projections to appropriately innervate target brain areas. J Neurosci. 2009;29(29):9137–47. https://doi.org/10.1523/jneurosci.5478-08.2009 PubMed PMID: 19625505; PubMed Central PMCID: PMCPMC6665563, Epub 2009/07/25.
2. Lefebvre JL, Kostadinov D, Chen WV, Maniatis T, Sanes JR. Protocadherins mediate dendritic self-avoidance in the mammalian nervous system. Nature. 2012;488(7412):517–21. https://doi.org/10.1038/nature11305 PubMed PMID: 22842903; PubMed Central PMCID: PMCPMC3427422, Epub 2012/07/31.
3. Chen WV, Nwakeze CL, Denny CA, O'Keeffe S, Rieger MA, Mountoufaris G, et al. Pcdhalphac2 is required for axonal tiling and assembly of serotonergic circuitries in mice. Science. 2017;356(6336):406–11. https://doi.org/10.1126/science.aal3231 PubMed PMID: 28450636; PubMed Central PMCID: PMCPMC5529183, Epub 2017/04/30.
4. Katori S, Noguchi-Katori Y, Okayama A, Kawamura Y, Luo W, Sakimura K, et al. Protocadherin-alphaC2 is required for diffuse projections of serotonergic axons. Sci Rep. 2017;7(1):15908. https://doi.org/10.1038/s41598-017-16120-y PubMed PMID: 29162883; PubMed Central PMCID: PMCPMC5698425, Epub 2017/11/23.
5. Mountoufaris G, Chen WV, Hirabayashi Y, O'Keeffe S, Chevee M, Nwakeze CL, et al. Multicluster Pcdh diversity is required for mouse olfactory neural circuit assembly. Science. 2017;356(6336):411–4. https://doi.org/10.1126/science.aai8801 PubMed PMID: 28450637; PubMed Central PMCID: PMCPMC5529182, Epub 2017/04/30.
6. Brasch J, Goodman KM, Noble AJ, Rapp M, Mannepalli S, Bahna F, et al. Visualization of clustered protocadherin neuronal self-recognition complexes. Nature. 2019;569(7755):280–3. https://doi.org/10.1038/s41586-019-1089-3 PubMed PMID: 30971825, Epub 2019/04/12.
7. Wu Q, Zhang T, Cheng JF, Kim Y, Grimwood J, Schmutz J, et al. Comparative DNA sequence analysis of mouse and human protocadherin

Asai *et al. Molecular Brain*　　(2020) 13:7

Page 9 of 10

gene clusters. Genome Res. 2001;11(3):389–404. https://doi.org/10.1101/gr.167301 PubMed PMID: 11230163; PubMed Central PMCID: PMCPMC311048. Epub 2001/03/07.

8. Thu CA, Chen WV, Rubinstein R, Chevee M, Wolcott HN, Felsovalyi KO, et al. Single-cell identity generated by combinatorial homophilic interactions between alpha, beta, and gamma protocadherins. Cell. 2014;158(5):1045–59. https://doi.org/10.1016/j.cell.2014.07.012 PubMed PMID: 25171406; PubMed Central PMCID: PMCPMC4183217. Epub 2014/08/30.

9. Molumby MJ, Keeler AB, Weiner JA. Homophilic Protocadherin Cell-Cell Interactions Promote Dendrite Complexity. Cell Rep. 2016;15(5):1037–50. https://doi.org/10.1016/j.celrep.2016.03.093 PubMed PMID: 27117416; PubMed Central PMCID: PMCPMC4856576. Epub 2016/04/28.

10. Wu Q, Maniatis T. A striking organization of a large family of human neural cadherin-like cell adhesion genes. Cell. 1999;97(6):779–90. https://doi.org/10.1016/s0092-8674(00)80789-8 PubMed PMID: 10380929. Epub 1999/06/25.

11. Hirano K, Kaneko R, Izawa T, Kawaguchi M, Kitsukawa T, Yagi T. Single-neuron diversity generated by Protocadherin-beta cluster in mouse central and peripheral nervous systems. Front Mol Neurosci. 2012;5:–90. https://doi.org/10.3389/fnmol.2012.00090 PubMed PMID: 22969705; PubMed Central PMCID: PMCPMC3431597. Epub 2012/09/13.

12. Hasegawa S, Kumagai M, Hagihara M, Nishimaru H, Hirano K, Kaneko R, et al. Distinct and Cooperative Functions for the Protocadherin-alpha, −beta and -gamma Clusters in Neuronal Survival and Axon Targeting. Front Mol Neurosci. 2016;9:155. https://doi.org/10.3389/fnmol.2016.00155 PubMed PMID: 28066179; PubMed Central PMCID: PMCPMC5179546. Epub 2017/01/10.

13. Malvache A, Reichinnek S, Villette V, Haimerl C, Cossart R. Awake hippocampal reactivations project onto orthogonal neuronal assemblies. Science. 2016;353(6305):1280–3. https://doi.org/10.1126/science.aaf3319 PubMed PMID: 27634534. Epub 2016/09/17.

14. Ghandour K, Ohkawa N, Fung CCA, Asai H, Saitoh Y, Takekawa T, et al. Orchestrated ensemble activities constitute a hippocampal memory engram. Nat Commun. 2019;10(1):2637. https://doi.org/10.1038/s41467-019-10683-2 PubMed PMID: 31201332; PubMed Central PMCID: PMCPMC6570652. Epub 2019/06/16.

15. Cobb SR, Buhl EH, Halasy K, Paulsen O, Somogyi P. Synchronization of neuronal activity in hippocampus by individual GABAergic interneurons. Nature. 1995;378(6552):75–8. https://doi.org/10.1038/378075a0 PubMed PMID: 7477292. Epub 1995/11/02.

16. Flossmann T, Kaas T, Rahmati V, Kiebel SJ, Witte OW, Holthoff K, et al. Somatostatin Interneurons Promote Neuronal Synchrony in the Neonatal Hippocampus. Cell Rep. 2019;26(12):3173–82.e5. https://doi.org/10.1016/j.celrep.2019.02.061 PubMed PMID: 30893591. Epub 2019/03/21.

17. Ghosh KK, Burns LD, Cocker ED, Nimmerjahn A, Ziv Y, Gamal AE, et al. Miniaturized integration of a fluorescence microscope. Nat Methods. 2011; 8(10):871–8. https://doi.org/10.1038/nmeth.1694 PubMed PMID: 21909102; PubMed Central PMCID: PMCPMC3810311. Epub 2011/09/13.

18. Ziv Y, Burns LD, Cocker ED, Hamel EO, Ghosh KK, Kitch LJ, et al. Long-term dynamics of CA1 hippocampal place codes. Nat Neurosci. 2013;16(3):264–6. https://doi.org/10.1038/nn.3329 PubMed PMID: 23396101; PubMed Central PMCID: PMCPMC3784308. Epub 2013/02/12.

19. Ohkawa N, Saitoh Y, Suzuki A, Tsujimura S, Murayama E, Kosugi S, et al. Artificial association of pre-stored information to generate a qualitatively new memory. Cell Rep. 2015;11(2):261–9. https://doi.org/10.1016/j.celrep.2015.03.017 PubMed PMID: 25843716. Epub 2015/04/07.

20. Kitamura T, Saitoh Y, Takashima N, Murayama A, Niibori Y, Ageta H, et al. Adult neurogenesis modulates the hippocampus-dependent period of associative fear memory. Cell. 2009;139(4):814–27. https://doi.org/10.1016/j.cell.2009.10.020 PubMed PMID: 19914173. Epub 2009/11/17.

21. Yagi T. Molecular codes for neuronal individuality and cell assembly in the brain. Front Mol Neurosci. 2012;5:45. https://doi.org/10.3389/fnmol.2012.00045 PubMed PMID: 22518100; PubMed Central PMCID: PMCPMC3324988. Epub 2012/04/21.

22. Hasegawa S, Kobayashi H, Kumagai M, Nishimaru H, Tarusawa E, Kanda H, et al. Clustered Protocadherins Are Required for Building Functional Neural Circuits. Front Mol Neurosci. 2017;10:114. https://doi.org/10.3389/fnmol.2017.00114 PubMed PMID: 28484370; PubMed Central PMCID: PMCPMC5401904. Epub 2017/05/10.

23. Fukuda E, Hamada S, Hasegawa S, Katori S, Sanbo M, Miyakawa T, et al. Down-regulation of protocadherin-alpha a isoforms in mice changes contextual fear conditioning and spatial working memory. Eur J Neurosci.

2008;28(7):1362–76. https://doi.org/10.1111/j.1460-9568.2008.06428.x PubMed PMID: 18973563. Epub 2008/11/01.

24. Yamagishi T, Yoshitake K, Kamatani D, Watanabe K, Tsukano H, Hishida R, et al. Molecular diversity of clustered protocadherin-alpha required for sensory integration and short-term memory in mice. Sci Rep. 2018;8(1):9616. https://doi.org/10.1038/s41598-018-28034-4 PubMed PMID: 29941942; PubMed Central PMCID: PMCPMC6018629. Epub 2018/06/27.

25. Liu X, Ramirez S, Pang PT, Puryear CB, Govindarajan A, Deisseroth K, et al. Optogenetic stimulation of a hippocampal engram activates fear memory recall. Nature. 2012;484(7394):381–5. https://doi.org/10.1038/nature11028 PubMed PMID: 22441246; PubMed Central PMCID: PMCPMC3331914. Epub 2012/03/24.

26. Carrillo-Reid L, Han S, Yang W, Akrouh A, Yuste R. Controlling Visually Guided Behavior by Holographic Recalling of Cortical Ensembles. Cell. 2019; 178(2):447–57.e5. https://doi.org/10.1016/j.cell.2019.05.045 PubMed PMID: 31257030; PubMed Central PMCID: PMCPMC6747687. Epub 2019/07/02.

27. Ohkura M, Sasaki T, Sadakari J, Gengyo-Ando K, Kagawa-Nagamura Y, Kobayashi C, et al. Genetically encoded green fluorescent Ca2+ indicators with improved detectability for neuronal Ca2+ signals. PLoS One. 2012; 7(12):e51286. https://doi.org/10.1371/journal.pone.0051286 PubMed PMID: 23240011; PubMed Central PMCID: PMCPMC3519846. Epub 2012/12/15.

28. Sato M, Kawano M, Ohkura M, Gengyo-Ando K, Nakai J, Hayashi Y. Generation and Imaging of Transgenic Mice that Express G-CaMP7 under a Tetracycline Response Element. PLoS One. 2015;10(5):e0125354. https://doi.org/10.1371/journal.pone.0125354 PubMed PMID: 25946002; PubMed Central PMCID: PMCPMC4422725. Epub 2015/05/07.

29. Li XG, Okada T, Kodera M, Nara Y, Takino N, Muramatsu C, et al. Viral-mediated temporally controlled dopamine production in a rat model of Parkinson disease. Mol Ther. 2006;13(1):160–6. https://doi.org/10.1016/j.ymthe.2005.08.009 PubMed PMID: 16182609. Epub 2005/09/27.

30. Iida A, Takino N, Miyauchi H, Shimazaki K, Muramatsu S. Systemic delivery of tyrosine-mutant AAV vectors results in robust transduction of neurons in adult mice. Biomed Res Int. 2013;2013:974819. https://doi.org/10.1155/2013/974819 PubMed PMID: 23762870; PubMed Central PMCID: PMCPMC3671507. Epub 2013/06/14.

31. Kawai S, Takagi Y, Kaneko S, Kurosawa T. Effect of three types of mixed anesthetic agents alternate to ketamine in mice. Exp Anim. 2011;60(5):481–7. https://doi.org/10.1538/expanim.60.481 PubMed PMID: 22041285. Epub 2011/11/02.

32. Barretto RP, Ko TH, Jung JC, Wang TJ, Capps G, Waters AC, et al. Time-lapse imaging of disease progression in deep brain areas using fluorescence microendoscopy. Nat Med. 2011;17(2):223–8. https://doi.org/10.1038/nm.2292 PubMed PMID: 21240263; PubMed Central PMCID: PMCPMC3833825. Epub 2011/01/18.

33. Kitamura T, Sun C, Martin J, Kitch LJ, Schnitzer MJ, Tonegawa S. Entorhinal Cortical Ocean Cells Encode Specific Contexts and Drive Context-Specific Fear Memory. Neuron. 2015;87(6):1317–31. https://doi.org/10.1016/j.neuron.2015.08.036 PubMed PMID: 26402611; PubMed Central PMCID: PMCPMC5094459. Epub 2015/09/25.

34. Takekawa T, Asai H, Ohkawa N, Nomoto M, Okubo-Suzuki R, Ghandour K, et al. Automatic sorting system for large calcium imaging data. bioRxiv. 2017:215145. https://doi.org/10.1101/215145.

35. Sato M, Mizuta K, Islam T, Kawano M, Takekawa T, Gomez-Dominguez D, et al. Dynamic embedding of salience coding in hippocampal spatial maps. bioRxiv. 2018:266767. https://doi.org/10.1101/266767.

36. Peyrache A, Benchenane K, Khamassi M, Wiener SI, Battaglia FP. Principal component analysis of ensemble recordings reveals cell assemblies at high temporal resolution. J Comput Neurosci. 2010;29(1):309–25. https://doi.org/10.1007/s10827-009-0154-6.

37. Lee D, Seung H. Algorithms for non-negative matrix factorization. Adv Neural Inf Proces Syst. 2001;13.

38. Lee DD, Seung HS. Learning the parts of objects by non-negative matrix factorization. Nature. 1999;401(6755):788–91. https://doi.org/10.1038/44565.

39. Arruda-Carvalho M, Sakaguchi M, Akers KG, Josselyn SA, Frankland PW. Posttraining ablation of adult-generated neurons degrades previously acquired memories. J Neurosci. 2011;31(42):15113–27. https://doi.org/10.1523/jneurosci.3432-11.2011 PubMed PMID: 22016545; PubMed Central PMCID: PMCPMC6623574. Epub 2011/10/22.

40. Arakawa T, Tanave A, Ikeuchi S, Takahashi A, Kakihara S, Kimura S, et al. A male-specific QTL for social interaction behavior in mice mapped with automated pattern detection by a hidden Markov model incorporated into

newly developed freeware. J Neurosci Methods. 2014;234:127–34. https://
doi.org/10.1016/j.jneumeth.2014.04.012 PubMed PMID: 24768576. Epub
2014/04/29.

41.   Kitamura T, Okubo-Suzuki R, Takashima N, Murayama A, Hino T, Nishizono H,
      et al. Hippocampal function is not required for the precision of remote
      place memory. Mol Brain. 2012;5(1):5. https://doi.org/10.1186/1756-6606-5-5.

Publisher's Note